JPEDAV (2004) 25:6-15
DOI: 10.1361/10549710417966
1547-7037/$19.00 ©ASM International

Comparison of Experimental and Simulated Multicomponent Ni-Base Superalloy Diffusion Couples

C.E. Campbell, J-C. Zhao, and M.F. Henry

(Submitted 19 December 2003)

A multicomponent diffusion mobility database for the Ni-rich fcc phase [2002Cam] is evaluated by comparing diffusion simulations to two experimental multicomponent Ni-base superalloy diffusion couples: Ni/René-88 and IN718/René-88. The diffusion simulations use composition-dependent thermodynamic and diffusion quantities within a finite difference code to simulate single-phase and multiphase planar layers. The multiphase layers consist of a matrix phase and a disperse phase. The calculated composition profiles, interdiffusion coefficients, phase fraction profiles, and location of Kirkendall porosity are compared with experimental results. To treat diffusion in the IN718 alloy, iron and carbon are added to the existing diffusion mobility database using previous assessment work and new assessments of Fe-Al and Fe-Co.

1. Introduction

The ability to optimize many industrial processes, such as casting and heat treating, requires the analysis of multicomponent diffusion. However, the modeling of multicomponent diffusion has been limited by the lack of multicomponent diffusion data. The recent development of a multicomponent diffusion database [2002Cam] for the face-centered-cubic (fcc) phase of Ni-rich alloys has provided the opportunity to model some of the issues associated with the processing and performance of Ni-base superalloys in the aerospace industry. In an effort to evaluate the diffusion mobility database, previous work compared diffusion simulations to experimental data for the René-N4/René-N5 diffusion couple [2003Cam]. The current work continues this evaluation of the diffusion mobility database by comparing the experimental results of two multicomponent diffusion couples of Ni/René-88 and René-88/IN718 to diffusion simulation predictions and suggesting areas where the database might be improved.

2. Background

Multicomponent diffusion simulations, using the DICTRA software [2000Bor, 2003DIC],[1] solve a system of coupled partial differential equations formed by combining flux and conservation equations. The partial differential equations are solved using a finite-difference method. Temperature and concentration-dependent diffusion coefficients are obtained from multicomponent thermodynamic factors and diffusion mobilities. Both the thermodynamic database and the diffusion mobility database are developed using a CALPHAD approach [1970Kau, 1998Sau] that enables the extrapolation to higher order systems based on the assessment of binary and ternary systems. The development and utilization of a mobility database relies on the pre-existence of a separate thermodynamic database for each phase of interest. For each phase, the thermodynamic database contains the assessments of the composition, temperature, and pressure-dependent Gibbs energies based on experimental phase diagram quantities and thermochemical data. With information from the thermodynamic database, the necessary thermodynamic factors can be used to convert the chemical potential gradients to concentration gradients. The thermodynamic database also determines the local equilibrium at each grid point during the simulation (i.e., whether the material is single phase or multiphase). The combined thermodynamic and diffusion mobility databases reproduce measured tracer, intrinsic, and chemical diffusion data, based on unary, binary, and ternary experimental data.

The diffusion mobility database is based on the formalism put forth by Ågren [1982Agr1, 1982Agr2] and Andersson and Ågren [1992And]. This formalism assumes a disordered solid solution with diffusion occurring by a vacancy exchange mechanism, in which the equilibrium vacancy concentration is maintained. The partial molar volumes of the substitutional species are assumed to be equal. Based on absolute-reaction rate theory, the mobility factor is defined as the product of a frequency factor and an activation enthalpy,

$$M_p = M_p^0 \frac{1}{RT} \exp\left(\frac{-Q_p^*}{RT}\right) \quad \text{(Eq 1)}$$

where M_p^0 represents the effects of the atomic jump distance (squared) and the jump frequency and has the units of (m^2/s). The variable Q_p^* is the diffusion activation enthalpy of species p in a given phase with units of (J/mol). The gas constant R is in (J/mol K) and the temperature T is in Kelvin. Both Q_p^* and M_p^0 are composition, temperature, and

C.E. Campbell, National Institute of Standards and Technology, Metallurgy Division, Gaithersburg, MD 20899-8555, and **J-C. Zhao** and **M.F. Henry,** General Electric Company, Global Research Ceramic and Metallurgy Technologies, P.O. Box 8, Schenectady, NY 12301. Contact e-mail: carelyn.campbell@nist.gov.

[1]The use of any commercial product does not constitute an endorsement by the National Institute Standards and Technology.

pressure dependent. Equation 1 can be simplified by using the empirical relation that the frequency factor M_p^0 is exponentially dependent on the composition. This was demonstrated by Kučera and Million [1970Kuc] and used by Jönsson [1994Jon] to reduce Eq 1 to the following:

$$M_p = \frac{1}{RT}\exp\left(\frac{-\Delta Q_p^*}{RT}\right) \quad \text{(Eq 2)}$$

where $\Delta Q_p^* = Q_p - RT\Theta_p$ and $M_p^0 = \exp(\Theta_p)$.

Ågren and coworkers [1992And, 1994Jön, 1995Jön, 1996Eng, 1999Hel1, 1999Hel2] expressed the composition and temperature dependence of each ΔG_p^* in terms of a Redlich-Kister [1948Red] polynomial, shown in Eq 3:

$$\Delta Q_p^* = \sum_j x_j A_i^j + \sum_q \sum_{j>q} x_q x_j \sum_k {}^k B_i^{qj} (x_q - x_j)^k. \quad \text{(Eq 3)}$$

A_i^j and ${}^kB_i^{qj}$ are linear functions of temperature. Note that for a given diffusing species i if all the A_i^j are equal and all the B_i^{qj} equal zero, then ΔQ_p^* and the corresponding M_p are not concentration dependent.

Optimized mobility functions for the Ni-Al-Co-Cr-Mo-Hf-Re-Ta-Ti-W system were obtained by Campbell [2002Cam] using the PARROT [1984Jan] optimization code. The composition and temperature dependence of ΔQ_p^* was determined using the available experimental diffusion tracer, intrinsic, and chemical diffusivity data. The experimental data were weighted giving preference to the tracer diffusivity D_p^* data, which are independent of concentration.

3. Experimental Procedure

Two diffusion couple experiments were performed using multicomponent diffusion couples of Ni/René-88 and René-88/IN718. The nominal compositions of the diffusion couple end members are given in Table 1. The diffusion couples were part of two diffusion multiples [2002Zha1, 2002Zha2], which are shown schematically in Fig. 1. Each diffusion multiple, 25 mm in length, consists of a 25 mm diameter cylinder with a 14 × 14 mm square opening into which four rectangular 7 × 7 × 25 mm bars were inserted. All of the sample pieces were cut using electro-discharge machining (EDM). The cut surfaces were then sand blasted with alumina particles under compressed air and cleaned using 600 grit SiC grinding paper to remove the EDM surface layer. Both diffusion multiples consisted of an outside cylinder of René-88. The rectangular inserts used in the first diffusion multiple consisted of Ni, Ta, W, and NiAl, and the second multiple contained the superalloys IN718, René-95, IN100, and ME3. The diffusion multiples were sealed by electron beam welding two René-88 disks, 25 mm in diameter and 3 mm in height on the top and bottom of each cylinder. Next, the welded assemblies underwent hot isostatic pressing (HIP) at 140 MPa, 1150 °C for 4 h. The HIPed diffusion multiples were encapsulated in an evacuated quartz tube and backfilled with argon. The encapsulated diffusion multiples were then heat-treated at 1150 °C for 1000 h followed by a water quench.

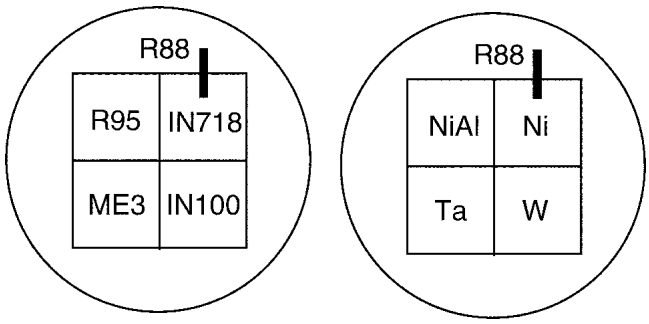

Fig. 1 Schematic diagram of the cross-sectional view of the diffusion multiples; see the text for their detailed size. The experimental data reported in this paper were taken from the René-88/IN718 and Ni/René-88 diffusion couples highlighted in this figure.

Table 1 Nominal Alloy Composition In Atomic Fraction (Mass Fraction)

	Ni	René-88	IN718
Ni	0.999	0.56 (0.56)	0.52 (0.53)
Al	…	0.045 (0.021)	0.011 (0.005)
Co	…	0.13 (0.13)	…
Cr	…	0.18 (0.16)	0.21 (0.19)
Fe	…	…	0.19 (0.185)
Mo	…	0.024 (0.04)	0.018 (0.03)
Nb	…	0.0044 (0.007)	0.032 (0.051)
Ti	…	0.045 (0.037)	0.011 (0.009)
W	…	0.013 (0.04)	…
C	…	0.0014 (0.0003)	0.0038 (0.0008)
B	…	0.0062 (0.00015)	…
Zr	…	0.0002 (0.0003)	…

The diffusion multiples were cut into two halves in a parallel orientation to the end cap disks. The cut surfaces were ground and polished. The polished samples were then analyzed using optical metallography and electron probe microanalysis (EPMA). Line scans were performed using EPMA analysis at 15 keV and 40 micro-amps using a CAMECA (Paris, France) microprobe. The carbon concentration was not measured during the EPMA analysis due to the concern that carbon buildup could occur during the line scans. The line scans are taken from the locations highlighted in Fig. 1 with bold lines. The result of other diffusion couples in the same diffusion multiples will be communicated separately.

The carbide phase fractions were measured using image analysis software, NIH ImageJ [2003Ras]. An optical micrograph revealing the carbide precipitation was analyzed by dividing the micrograph into 100 × 1750 μm sections starting from the initial bond interface. For each section, the precipitate fraction was calculated as the sum of the second-phase particle area divided by the total area of the section. For comparison with the simulation predictions, the area fraction was converted to a mole fraction using a ratio of an average Ti,Nb-based MC carbide (MC is a fcc metal carbide where M = Ti,Nb) and Ni-base γ molar volumes. The

molar volumes are calculated based on the lattice parameters published by Wlodek et al. [1996Wlo].

4. Diffusion Simulations

DICTRA was used to simulate the various diffusion couples using the Ni-Data thermodynamic database [1996Sau] and the Ni diffusion mobility database [2002Cam]. All of the simulations assumed a 4 mm length for each side of the couple and used a geometric grid that placed a higher number of points at the interface between the two end-members. An initial comparison of a simulation that included the heating and cooling of the diffusion couple to a simulation that included only the isothermal diffusion hold showed only insignificant differences in the calculated composition profiles. Thus, the diffusion simulations considered only diffusion that occurred during the isothermal diffusion holds and did not consider any diffusion that may have occurred during heating or cooling. The initial compositions of the diffusion couples are the nominal alloy compositions listed in Table 1. The diffusion simulations did not include boron (B) or zirconium (Zr). Equilibrium calculations at 1150 °C, shown in Table 2, predicted a small fraction (less than 1%) of MC carbide present in both René-88 and IN718. The small fraction MC carbide predicted in René-88 was not included in the Ni/René-88 diffusion couple simulation, as the predicted equilibrium mole fraction was less than 0.005. Thus, the Ni/René-88 diffusion couple is treated as a metastable local equilibrium with respect to the formation of the MC carbide.

In contrast to the equilibrium calculations for René-88, the predicted equilibrium mole fraction of the MC carbide for IN718 at 1150 °C is greater than 0.005; thus the René-88/IN718 diffusion simulation does include the MC carbide and uses the dispersed phase model within the DICTRA code [1994Eng]. As applied in this simulation, the dispersed phase model assumes that the fcc phase exists as a continuous phase (the matrix) and that diffusion occurs only in the matrix phase. The MC carbide is chosen as a dispersed phase and acts as point sinks or sources for solute atoms as the carbide grows or shrinks in response to the local matrix composition. Specifically, at each grid node and after each time step, the equilibrium fractions and compositions of γ and MC carbide are calculated, and thus it is assumed that local equilibrium is achieved.

4.1 Expansion of Diffusion Database

For comparison with the current experimental work, Fe and C must be added to the diffusion mobility database. Iron was added using the previous assessments of Fe-Ni-Cr [1995Jön] and assessments of the Fe-Al and Fe-Co systems. Experimental tracer diffusivity data of Fe into Al were used to assess the mobility functions of Fe in Al [1970Hoo, 1971Tiw, 1987Bek]. All of the experimental work was below the melting temperature of Al (933 K); thus, the extrapolations to higher temperatures should be used with caution. For the available data, the Fe mobility parameters were assessed, and the values are given in Table 3. Figure 2 shows the tracer diffusivity of Fe in Al as a function of temperature. Unfortunately, there were not enough data available to assess the mobility of Al in Fe; so the mobility of Al into Ni, as assessed by Engström and Ågren [1996Eng], was used as an estimate.

Table 2 Calculated Equilibrium Phase Fractions at 1150 °C

Alloy	Phase Fraction MC carbide
Ni	…
René-88	0.0027
IN718	0.0081

Table 3 Diffusion Mobility Parameters for Fe-Al and Fe-Co

Parameter		Value	Reference
Mobility of Al			
MQ(fcc,Al:VA;0)	A_{Al}^{Al}	−142000-72.11*T	[1996Eng]
MQ(fcc,Fe:VA;0)	A_{Al}^{Fe}	−284000-59.83*T	[1996Eng]
Mobility of Co			
MQ(fcc,Co:VA;0)	A_{Co}^{Co}	−286175-75.98*T	[2002Cam]
MQ(fcc,Fe:VA;0)	A_{Co}^{Fe}	−288100-79.51*T	This work
MQ(fcc,Fe,Co:VA;0)	${}^{0}B_{Co}^{Co,Fe}$	+120800-97.61*T	This work
Mobility of Fe			
MQ(fcc,Al:VA;0)	A_{Fe}^{Al}	−168760-63.54*T	This work
MQ(fcc,Co:VA;0)	A_{Fe}^{Co}	−251000-94.13*T	This work
MQ(fcc,Fe:VA;0)	A_{Fe}^{Fe}	−286000-79.54*T	[1995Jön]
MQ(fcc,Al,Fe:VA;0)	${}^{0}B_{Fe}^{Al,Fe}$	+266220-5.11*T	This work
MQ(fcc,Co,Fe:VA;0)	${}^{0}B_{Fe}^{Co,Fe}$	+208100-104.7*T	This work

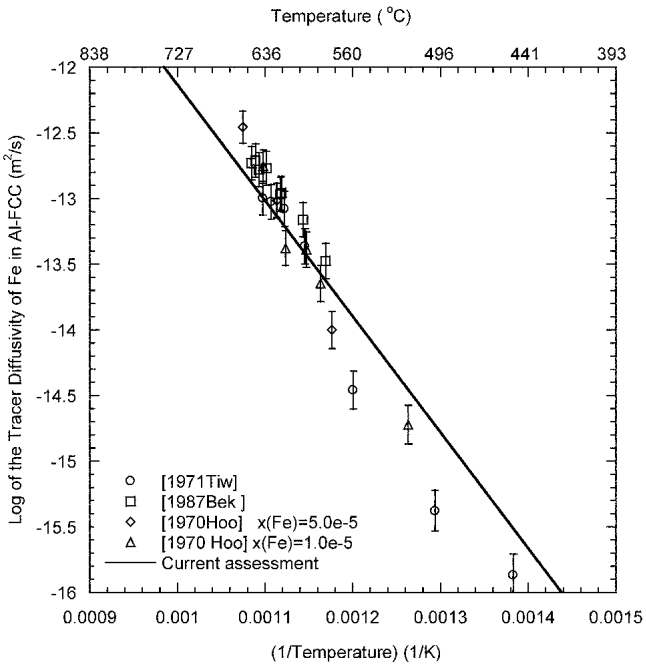

Fig. 2 Experimental and calculated tracer diffusivity of Fe in Al-fcc as a function of temperature; symbols represent experimental work and the solid line is the calculation.

The diffusion mobility of Co in fcc-Fe was assessed using experimental tracer diffusivity data and interdiffusion coefficients. Hirano and Cohen [1972Hir] measured the tracer diffusivity of Co in Fe in the temperature range 1223 K to 1583 K for Co compositions ranging from 1.0×10^{-6} to 0.896 weight fraction. Ustad and Sørum [1973Ust] determined the interdiffusion coefficients for the entire Fe-Co composition range in the temperature range from 1273 to 1673 K. Using these experimental data and weighting the tracer diffusivity data higher than the interdiffusion coefficient data, the Co-Fe mobility parameters were determined using the PARROT optimizer within DICTRA. Below 1273 K, it was noted that grain boundary diffusion contributed significantly, thus these low temperature data were not used for the assessment. The assessed mobility parameters are given in Table 3. Figure 3(a) compares the calculated diffusivity with the experimental Co tracer diffusivity data measured by Hirano and Cohen [1972Hir]. Figure 3(b) shows the calculated and measured interdiffusion coefficients [1973Ust].

The mobility of Fe in the fcc phase of the remaining elements (Mo, Nb, Ti, W) was estimated based on the previous assessed mobility of Ni [Cam2002], as Fe and Ni have similar atomic masses and atomic radii. That is, the mobility parameters for Fe diffusion in fcc Mo, Nb. Ti, and W were set equal to the mobility parameters determined for Ni. These simplified estimates are not ideal; however, the diffusion data for the fcc structure of the above elements into fcc Fe is limited.

Interstitial elements can be added to the database by using a sublattice description and by assuming the partial molar volume of the interstitial element is zero [1982Agr2]. Carbon was added to the mobility database by using the Fe-Ni-Cr-C assessment for the fcc phase by Jönsson [1994Jon] and by estimating the C mobility in the remaining elements in the database. These simplified estimates were based on the likeness of the element to Fe, Ni or Cr and then assuming the mobility of C was the same as in Fe, Ni, or Cr. The remaining elements were grouped as follows: Co grouped with Fe; Al grouped with Ni; and Mo, W, Nb, and Ti grouped with Cr. It is acknowledged that this estimation method is not ideal; however, for the small amount of C present in the fcc phase of the Ni-rich alloys this method should be sufficient.

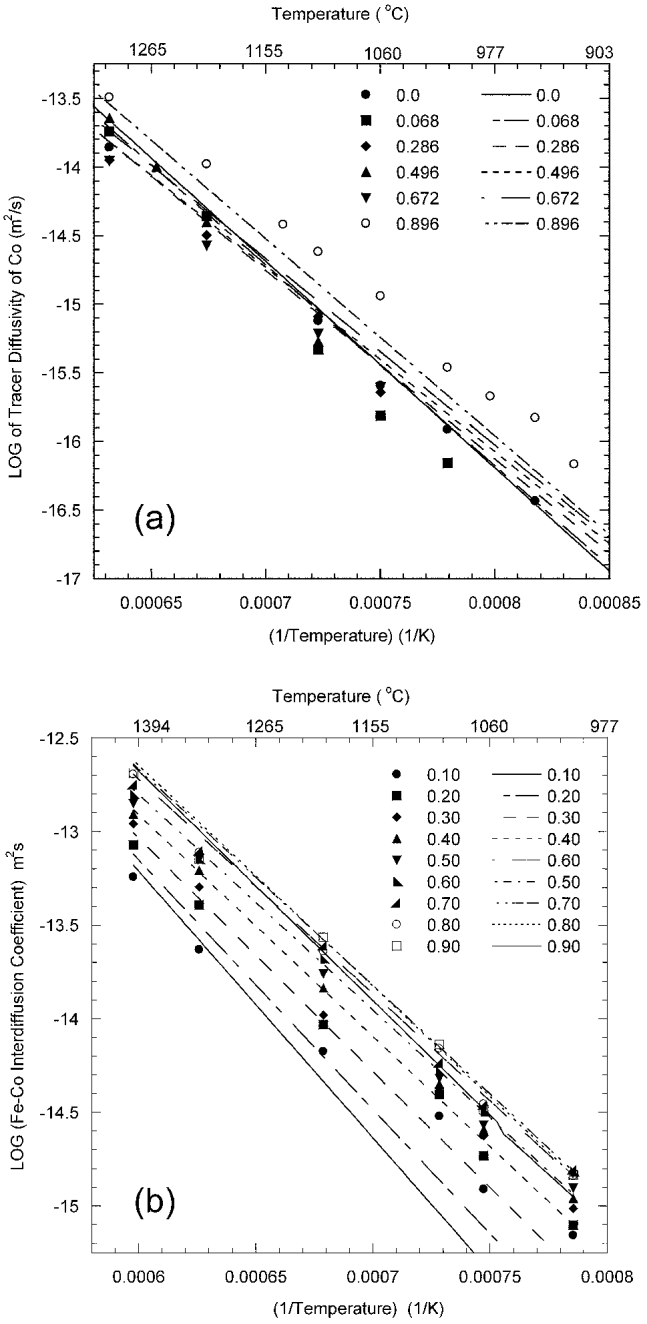

Fig. 3 **(a)** Tracer diffusivity of Co in Fe-FCC as function of inverse temperature for various levels of Co concentration; experimental data are from Hirano and Cohen [1972Hir]. **(b)** Interdiffusion coefficient for Co-Fe for various Co-Fe alloys as a function of inverse temperature; the experimental data are from Ustad and Sørum [1973Ust]. The symbols represent the experimental data and the lines the calculation. The legends show the atomic fraction of Co.

5. Results and Comparisons

5.1 Methods of Comparison

The multicomponent diffusion mobility database was evaluated by comparing the diffusion simulation results to the experimental diffusion couple results. The evaluation includes the comparison of composition and phase fraction profiles, interdiffusion coefficients, and the location of Kirkendall porosity. To compare the experimental and calculated composition profiles, a Matano plane for the experimental diffusion couple must be defined and then equated to the zero grid position of the calculated profiles. The Matano plane for the couple is taken as the average of the Matano planes for each of the experimental composition profiles. The differences between the Matano planes calculated for the experimental composition profiles indicate the degree of inconsistency in the experimental measurements.

Once a common grid reference is defined for plotting the experimental and calculated concentration profiles, a simple error analysis is conducted for each of the element concentration profiles. The average error for each profile was calculated using the following:

$$\text{Average Error} = \frac{1}{n}\sum_{1}^{n}\left|x_i^{exp} - x_i^{cal}\right| \quad \text{(Eq 4)}$$

where n is the number of grid points and x_i^{exp} and x_i^{cal} are the experimental and calculated concentration values at each grid point, respectively. The errors for each element were normalized by dividing the error by the average of the end-member concentrations.

From a single multicomponent experimental diffusion couple it is not possible to directly determine the interdiffusion coefficients to compare with the calculations; however, Dayananda and Sohn [1996Day1,1996Day2] have proposed a method to determine the experimental average effective interdiffusion coefficients. This method integrates the interdiffusion flux of a component over the diffusion distance of a selected range of compositions. In this method, the average effective diffusion coefficients for each side of the diffusion couples are compared with averaged calculated diagonal interdiffusion coefficients obtained from the simulation. The averaged calculated diagonal interdiffusion coefficients from the simulations are taken as the average of 12 interdiffusion coefficients calculated for specific compositions on a given side of the diffusion couple. This comparison should be viewed with caution as the experimental method for determining the average effective diffusion coefficient assumes that the off-diagonal terms in the interdiffusion coefficient matrix are negligible. The interdiffusion coefficient matrix calculated for this work indicates that the off-diagonal terms can be significant.

In many diffusion couples, a region of porosity may develop if sufficient vacancy sinks are not available (i.e., vacancy annihilation is slow). This porosity is generally referred to as Kirkendall porosity and is observed on the side of the diffusion couple with the faster diffusing elements in the lattice-fixed frame of reference. It is possible to compare the location of any observed Kirkendall porosity to that predicted by the diffusion simulations. The simulations assume that in the lattice-fixed frame of reference, the sum of the net atom fluxes equals the vacancy flux. The negative divergence of the vacancy flux ($-\nabla \cdot J_{Va}$) gives the number of sinks (sources) necessary to maintain local equilibrium. Thus, the predicted location of the Kirkendall porosity is given by the largest negative value of the vacancy flux gradient, as demonstrated by Höglund and Ågren [2001Hog].

5.2 Ni/René-88

The calculated equilibrium state for both Ni and René-88 at 1150 °C is single phase fcc. Optical metallography shown in Fig. 4 indicates a smooth bond between the two alloys and some porosity near the initial interface. At a higher magnification, a small fraction of MC carbides was observed on the René-88 side of the couple. This fraction was below the resolution of the current measurement technique. The solid line in Fig. 4 indicates the position of the initial interface. Figure 5 shows the experimental and calculated concentration profiles for the 1000 h diffusion couple. The Matano interface for the couple, based on the Al, Co, Cr, Mo, and W concentration profiles, was equated to the corresponding initial interface between Ni/René-88 defined in the simulations. The standard deviation from the averaged Matano interface for the couple was 25 μm. This deviation is acceptable as it is less than 5% of the average diffusion distance of 750 μm. Figure 5(a) shows the calculated profiles for the major alloying additions of René-88, Co and Cr, and Fig. 5(b) shows the profiles for the alloying additions that are less than 0.05 mass fraction. The calculated W, Mo, and Nb profiles are in agreement with the experiment; however, comparison of the Ti and Al profiles indicates substantial discrepancies. The calculated Ti concentration is higher than the measured concentration on the Ni-rich side of the couple and is lower than the measured concentration on the René-88 side of the couple. This implies that the calculated Ti diffusion is faster than that observed in the experiment and that the observed non-monotonic behavior is less than that calculated. The calculated Al profile is more non-monotonic than the measured Al profile.

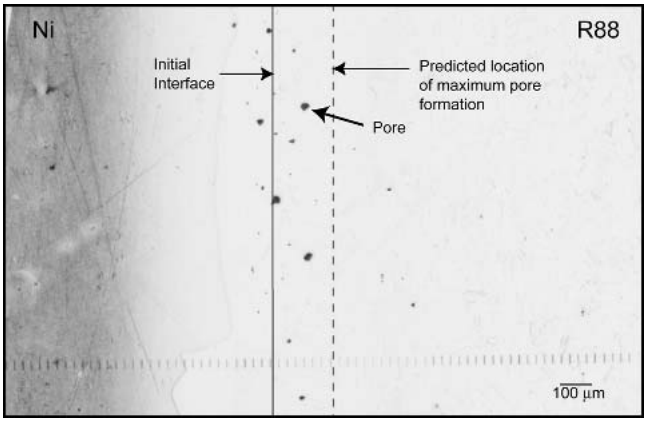

Fig. 4 Optical micrograph of Ni/René-88 diffusion couple after 1000 h at 1150 °C. The solid line indicates the position of the initial interface. The dashed line shows the position of the predicted maximum pore formation.

The results of the simple error analysis for each profile on the René-88-side are given in Table 4. The largest average error was associated with the Ti concentration profile (0.42%) and the smallest average error was associated with the Mo profile (0.11%). The large average and normalized error for Ti is in agreement with the discrepancies seen in Fig. 5(b). The large normalized error for Nb (34%) is not observed in Fig. 5(b). This large normalized error is due to small concentration of Nb in René-88, which is less than 0.01 mass fraction.

Table 5 compares the calculated average interdiffusion coefficients and the end-member compositions to the average effective diffusion coefficients determined from the experimental couple using the method of Dayanada and Sohn

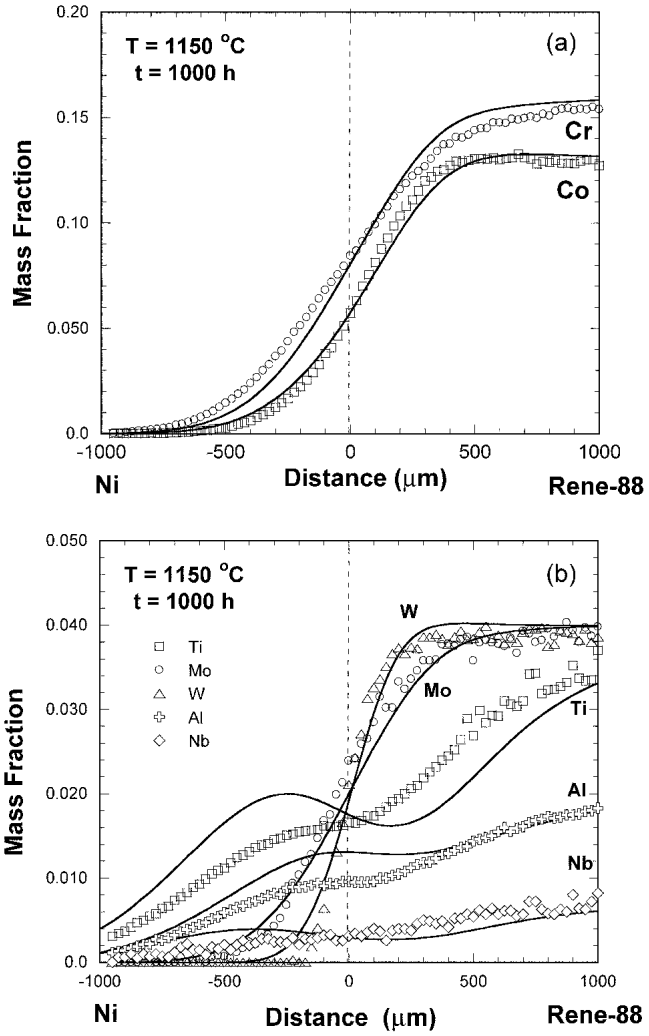

Fig. 5 Calculated and experimental concentration profiles for the Ni/René-88 diffusion couple at 1150 °C for 100 h. Calculated profiles are represented by lines and the experimental profiles measured using EPMA are represented by symbols. **(a)** Co and Cr composition profiles. **(b)** Al, Mo, Nb, Ti, and W concentration profiles.

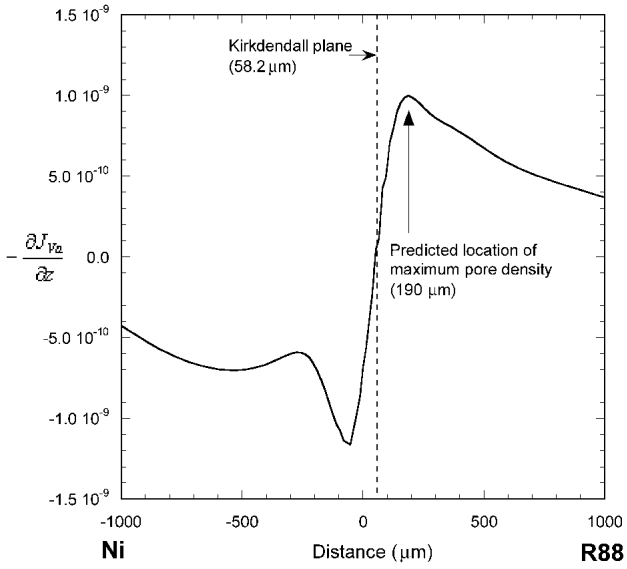

Fig. 6 Predicted maximum pore density for Ni/René-88 couple after 1000 h at 1150 °C. The dashed line is the calculated position of the Kirkendall plane after 1000 h.

Table 4 Average Error for Ni/René-88 Composition Profiles

Element	Max Error $\lvert x_i^{exp} - x_i^{cal}\rvert_{max}$, wt.%	Average Error $\frac{1}{n}\sum_{1}^{n}\lvert x_i^{exp} - x_i^{cal}\rvert$, wt.%	Standard Deviation of the error, wt.%	Normalized Average Error, wt.%
Al	0.44	0.17	±0.16	16
Co	0.79	0.33	±0.24	5.1
Cr	0.98	0.30	±0.21	3.8
Mo	0.29	0.11	±0.09	5.5
Nb	0.20	0.12	±0.05	34
Ti	0.79	0.42	±0.22	23
W	0.51	0.14	±0.14	7

Table 5 Comparison of Interdiffusion Coefficients (m^2/s) for Ni/René-88 after 1000 h

	Ni Average Effective (Exp)	Calculated Average	Calculated for Ni	Calculated at the Center	R88 Average Effective (Exp)	Calculated Average	Calculated for R88
Al	5.0×10^{-14}	3.53×10^{-14}	2.82×10^{-14}	4.02×10^{-14}	7.53×10^{-14}	5.80×10^{-14}	9.85×10^{-14}
Co	7.66×10^{-15}	1.23×10^{-14}	1.09×10^{-14}	1.24×10^{-14}	7.65×10^{-15}	1.08×10^{-14}	1.07×10^{-14}
Cr	1.91×10^{-14}	1.29×10^{-14}	1.26×10^{-14}	1.31×10^{-14}	2.57×10^{-15}	1.19×10^{-14}	1.09×10^{-14}
Mo	9.54×10^{-15}	1.06×10^{-14}	1.06×10^{-14}	1.05×10^{-14}	1.52×10^{-14}	9.92×10^{-15}	9.33×10^{-15}
Nb	5.08×10^{-14}	3.40×10^{-14}	3.23×10^{-14}	3.38×10^{-14}	4.17×10^{-14}	3.37×10^{-14}	3.43×10^{-14}
Ti	5.79×10^{-14}	3.97×10^{-14}	3.20×10^{-14}	3.91×10^{-14}	5.39×10^{-14}	4.06×10^{-14}	4.44×10^{-14}
W	1.17×10^{-15}	3.06×10^{-15}	1.23×10^{-15}	2.64×10^{-15}	1.14×10^{-14}	1.56×10^{-14}	5.48×10^{-15}

[1996Day1,1996Day2]. The experimentally assessed interdiffusion coefficients and the calculated diffusion coefficients are within a factor of 2, which is a reasonable agreement considering the error associated with the experimental method.

Experimental observations and predictions of the loca-

tion of the Kirkendall porosity are in qualitative agreement. Figure 4 indicates some porosity near the initial interface and primarily on the René-88 side of the diffusion couple. The diffusion simulations predict the maximum $-\nabla \cdot J_{Va}$ at 190 μm to the right of the initial interface on the René-88 side of the diffusion couple. This result is shown in Fig. 6 as a plot of the negative divergence of the vacancy flux ($-\nabla \cdot J_{Va}$) as a function of distance. The position of maximum pore formation predicted by the simulation is shown in Fig. 4 as a dashed line and is in qualitative agreement with the experiment. The Kirkendall plane is 58 μm to the right of the initial interface on the René-88 side of the couple.

5.3 René-88/IN718

The equilibrium phase distributions of René-88 and IN718 are given in Table 2. At 1150 °C, IN718 has a small equilibrium fraction of MC (M = Nb, Ti) carbide, less than 1%. Figure 7 shows a micrograph of the René-88/IN718 after 1000 h at 1150 °C, with significant carbide precipitation on the IN718 side of the couple and a small fraction of carbide precipitation on the René-88 side. The initial interface is in the center of the micrograph, as indicated by the dashed line. The Matano interface for the couple was defined as the average of the Matano interfaces calculated from the experimental Co, Cr, Fe, Mo, and W concentration profiles. The standard deviation from the Matano interface for the couple was 50 μm, with the Cr interface having the largest deviation of 100 μm. This deviation is less than ideal as it is 10% of the average diffusion distance of 750 μm. Unfortunately, the ability to repeat the measurement of the concentration profiles was not available and the current experimental data were accepted.

Figure 8 compares the predicted MC carbide phase fraction profile to the measured carbide fraction after 1000 h on the IN718 side of the couple. The fraction of carbides on the René-88 side of the couple is too small to measure with the current measurement technique. Experimentally, the MC carbide precipitates form 247 μm to the right of the initial interface. The DICTRA simulation also predicted the MC carbide precipitation on the IN718 side after 1000 h; however, the simulations predicted the formation of a sharp carbide peak (with a width equal to 80 μm) near the initial interface, followed by a carbide free zone with a width of 200 μm, and a broad carbide peak and plateau. The calculated broad carbide peak, with a maximum of 0.0145 mol phase fraction, is similar to the experimental measurements that show a sharp increase to a plateau of approximately 0.02 mol phase fraction at 247 μm.

Figure 9 compares the experimental and calculated fcc concentration profiles. The experimental and calculated Co, Fe, Al, Ti, and Mo concentration profiles are in agreement. The experimental and calculated Cr profiles are also in agreement on the René-88 side of the couple; however, on the IN718 side of the couple the experimental Cr concentration is consistently less than predicted. This discrepancy could be the result of the actual end-member concentration being lower than reported. Comparison of the experimental and calculated W profiles suggest that the W diffused more quickly than predicted; the experimental diffusion distance is greater than the predicted distance. The experimental and calculated Nb profiles show the largest discrepancies for the concentration profiles. The experimental Nb profile is consistently lower than the predicted profile; however, the shapes of the experimental and predicted profiles are similar. This indicates that actual alloy Nb concentrations may be lower than the reported nominal concentration.

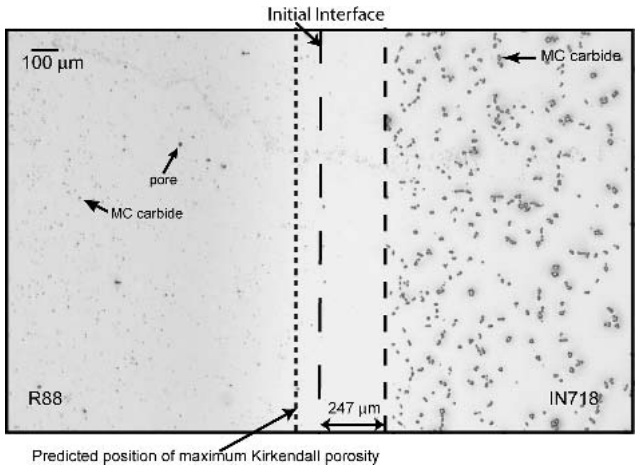

Fig. 7 Optical micrograph of Rene88/IN718 diffusion couple after 1000 h at 1150 °C. MC carbides are visible on the IN718 side of the couple. There is a carbide free zone between the initial interface and the two phase region of MC carbide and γ on the IN718 side.

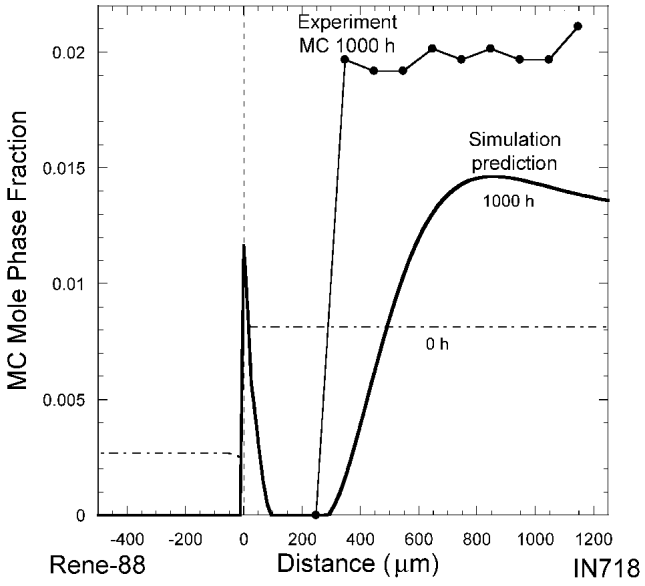

Fig. 8 Calculated and measured MC carbide profiles as function of distance for the René-88/IN718 diffusion couple at 1150 °C for 1000 h. The initial predicted, carbide phase fraction is represented by the dashed line, the predicted fraction after 1000 h is given by the solid line, and the symbols represent the experimental data points.

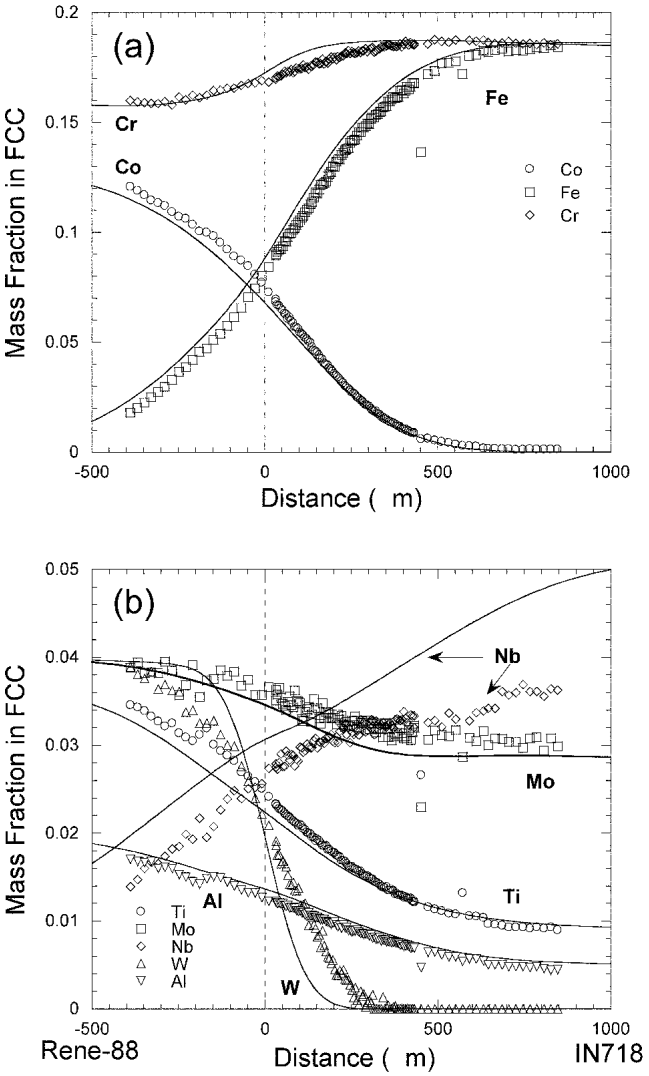

Fig. 9 The calculated and experimental concentration profiles for the René-88/IN718 diffusion couple at 1150 °C for 1000 h. Calculated profiles are represented by lines and the experimental profiles measured using EPMA are represented by symbols. **(a)** Co, Cr and Fe composition profiles. **(b)** Al, Mo, Nb, Ti, and W concentration profiles.

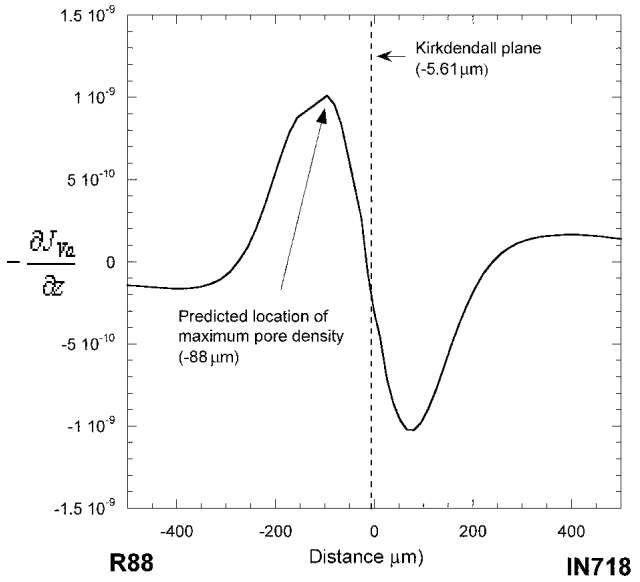

Fig. 10 Predicted maximum pore density for René-88/IN718 after 1000 h at 1150 °C; the dashed line is the calculated position of the Kirkendall plane after 1000 h.

Table 6 Average Absolute Error for René-88/IN718 Composition Profiles

Element	Max Error $\lvert x_i^{exp} - x_i^{cal}\rvert_{max}$, wt.%	Average Error $\frac{1}{n}\sum_{1}^{n} \lvert x_i^{exp} - x_i^{cal}\rvert$, wt.%	Standard Deviation of the Error, wt.%	Normalized Average Error, wt.%
Al	0.28	0.12	±0.08	9.2
Co	0.97	0.47	±0.31	7.2
Cr	1.1	0.40	±0.34	2.3
Fe	1.47	0.69	±0.44	7.5
Mo	0.16	0.08	±0.04	2.3
Nb	4.92	0.73	±0.51	25.2
Ti	0.24	0.15	±0.77	6.5
W	0.36	0.16	±0.11	78.0

Simple error analysis of the differences between the experimental and calculated concentration profiles given in Table 6 agrees with observations made on reviewing Fig. 9. The error analysis also indicates that in general the experimental and predicted concentration profiles are in agreement with the experimental measurement, as the average errors are all less than 1%. The largest average error (0.73%) is associated with the Nb concentration profile. The smallest average error (0.08%) is associated with the Mo concentration profile. The normalized average errors also indicate that Nb has the largest disagreement with the experiment with a normalized average error of 25%.

Table 7 shows a comparison of calculated average and estimated experimental average effective diagonal interdiffusion coefficients. The experimental diffusion coefficients represent the effective interdiffusion coefficient on either the René-88 side or the IN718 side. The calculated IN718 and experimental average effective IN718 interdiffusion coefficients are within a factor of 2. On the René-88 side, comparison of the calculated and experimental average effective interdiffusion coefficients shows some significant differences: the diagonal Al, Cr, Nb, Ti, and W coefficients differ by a factor of 10. The large discrepancy for the Nb interdiffusion coefficient is not unexpected given the differences observed in the experimental and calculated concentration profiles (Fig. 9b). The significantly fewer experimental concentration points on the René-88 side of the profiles and that for some of the concentration profiles the data did not extend the entire diffusion distance may have contributed to a larger experimental error for the René-88 diffusion coefficients.

Table 7 Comparison of Interdiffusion Coefficients (m^2/s) for René-88/IN718 after 1000 h

	R88 Average Effective (Exp)	Calculated Average	Calculated for R88	Calculated at the Center	IN718 Average Effective (Exp)	Calculated Average IN718	Calculated for IN718
Al	5.89×10^{-15}	6.58×10^{-14}	9.49×10^{-14}	4.70×10^{-14}	1.36×10^{-14}	2.96×10^{-14}	2.15×10^{-14}
Co	9.41×10^{-15}	1.01×10^{-14}	1.08×10^{-14}	9.91×10^{-15}	1.28×10^{-14}	9.17×10^{-15}	8.57×10^{-15}
Cr	1.92×10^{-15}	1.12×10^{-14}	1.12×10^{-14}	1.17×10^{-14}	1.58×10^{-14}	1.16×10^{-14}	1.07×10^{-14}
Fe	3.87×10^{-15}	1.65×10^{-14}	1.72×10^{-14}	1.43×10^{-14}	1.56×10^{-14}	1.09×10^{-14}	8.89×10^{-15}
Mo	3.61×10^{-15}	9.55×10^{-15}	9.36×10^{-15}	9.73×10^{-15}	1.66×10^{-14}	9.99×10^{-15}	1.01×10^{-14}
Nb	4.11×10^{-15}	3.27×10^{-14}	2.75×10^{-14}	3.58×10^{-14}	6.69×10^{-14}	3.99×10^{-14}	4.27×10^{-14}
Ti	4.48×10^{-15}	4.21×10^{-14}	4.46×10^{-14}	3.97×10^{-14}	2.02×10^{-14}	3.68×10^{-14}	3.68×10^{-14}
W	3.02×10^{-15}	9.57×10^{-16}	8.27×10^{-16}	1.11×10^{-15}	3.77×10^{-15}	1.21×10^{-15}	1.23×10^{-15}

The experimental observations (Fig. 7), indicate some porosity on the René-88 side of the couple, in qualitative agreement with the diffusion simulations. For the René-88/IN718 couple, the calculated position of maximum pore formation is 88 μm to the left of the initial interface, as shown in Fig. 10. The Kirkendall plane, after 1000 h at 1150 °C, is 5.6 μm to the left of the original interface.

Overall, the comparison of the experimental diffusion couples to the diffusion simulations showed good agreement, indicating the multicomponent diffusion mobility database, based on binary and ternary interactions, extrapolates well to the higher order Ni-rich systems. The discrepancies that exist between the experimental and calculated profiles are the result of both experimental uncertainties and simulation assumptions. Experimental uncertainties include the possible discrepancies between the reported nominal alloy composition and the actual end-member compositions. This discrepancy is most apparent in the Nb concentration profile of the René-88/IN718 diffusion couple. Another experimental uncertainty is the carbide formation, which adds to the experimental scatter in the matrix composition profiles, especially in the IN718 alloy. The simulations rely on a diffusion mobility database that includes primarily Ni-binary interactions with some Ni-base ternary interactions. It is possible that high order interactions may make small contributions to error in the diffusion simulations; however, without the necessary experimental data to evaluate these interactions the discrepancies are accepted and expected to be negligible. As the diffusion simulations are based on both a multicomponent thermodynamic database and a diffusion mobility database, assumptions used in the thermodynamic database may also contribute to discrepancies between the diffusion simulations and experiments.

The analysis of two diffusion couple experiments does suggest that further improvements may be made by reassessment of some of the binary systems.

The Ni/René-88 couple comparisons suggested Ni-Al and Ni-Ti interactions might require revision, while the René-88/IN718 couple comparisons indicated that the Ni-Al, Ni-Nb, and Ni-W interactions may require some revision. While the diffusion mobility database parameters could be modified to fit each individual diffusion couple profile, the purpose of the database is to represent the entire composition space. Thus, additional experimental evaluations of other multicomponent diffusion couples will help to determine which and how the mobility parameters should be modified to best represent composition-dependent diffusivities.

6. Summary

Two multicomponent diffusion couples (Ni/René-88 and René-88/IN718) were simulated using a multicomponent thermodynamic database and a multicomponent diffusion mobility database in conjunction with a finite-difference diffusion code. Iron was added to the mobility database using previous mobility assessments and the present assessments of Fe-Al and Fe-Co in the fcc phase. While the Fe addition was added specifically to allow modeling of the IN718 alloy, the addition can be used to simulate any Ni-rich alloy with Fe. Carbon was also added to the database based on previous assessment work and simplifying assumptions for the binary interactions.

To evaluate the accuracy of the diffusion mobility database, the diffusion simulations were compared with experimental results using composition profiles, the Kirkendall porosity location, and diffusion coefficients. Overall, the calculated and experimental composition profiles are in quantitative agreement. The differences between the calculated and measured composition profiles and interdiffusion coefficients are within the experimental uncertainty. The diffusion simulations correctly predicted the formation the MC carbide on the IN718 side of the René-88/IN718 couple. The predicted location of maximum pore formation was also in qualitative agreement with the location of the observed pores.

Analysis of the two multicomponent diffusion couples suggests that improvements may be made to the Ni-Al, Ni-Nb, Ni-Ti, and Ni-W interactions. However, before the binary interactions are modified, additional experimental evaluations are needed to evaluate possible higher order interaction contributions. Overall, the current comparison of two Ni-base superalloy diffusion couple experiments to diffusion simulations demonstrates the potential of using multicomponent thermodynamics and diffusion mobility databases to model multicomponent diffusion behavior in complex alloys.

Acknowledgment

This work was supported by the Defense Advanced Research Project Agency (DARPA) under the accelerated Insertion of Materials (AIM) program (Grant No. F33615-00-C-5215) with Dr. L. Christodoulou as the project manager and Dr. Rollie Dutton as the project monitor. The authors would like to express their appreciation to N. Saunders for the use of his thermodynamic database for Ni alloys. The authors are also grateful for the helpful discussions with W.J. Boettinger while reviewing this paper.

References

1948Red: O. Redlich and A. Kister: "Algebraic Representation of Thermodynamic Properties and the Classification of Solutions," *Ind. Eng. Chem.,* 1948, *40,* p. 345.

1970Hoo: G. M. Hood: "The Diffusion of Iron in Aluminum," *Philos. Mag.,* 1970, *21*(169), pp. 305-28.

1970Kau: L. Kaufman and H. Bernstein, *Computer Calculation of Phase Diagrams*, Academic Press, London, 1970.

1970Kuc: J. Kučera and B. Million: "Self-Diffusion in Substitutional Solid Solutions With Fcc Lattice," *Metall. Trans. A,* 1970, *1,* pp. 2603-2606.

1971Tiw: G. P. Tiwari and B. D. Sharma: "Diffusion of Iron in Aluminum," *Philos. Mag.,* 1971, *24*(189), pp. 739-43.

1972Hir: K-I. Hirano and M. Cohen: "Diffusion of Cobalt in Iron-Cobalt Alloys," *Trans. JIM,* 1972, *13*(2), pp. 96-102.

1973Ust: T. Ustad and H. Sørum: "Interdiffusion in the Fe-Ni, Ni-Co and Fe-Co Systems," *Phys. Status Solidus A,* 1973, *20* pp. 285-94.

1982 Agr1: J. Ågren: "Numerical Treatment of Diffusional Reactions in Multicomponent Alloys," *J. Phys. Chem. Solids,* 1982, *43*(4), pp. 385-91.

1982Agr2: J. Ågren "Diffusion in Phases with Several Components and Sublattices," *J. Phys. Chem. Solids,* 1982, *43*(5), pp. 421-30.

1984Jan: B. Jansson, Parrot-Optimizer, Royal Institute of Technology, Stockholm, Sweden, 1984.

1987Bek: D. L. Beke, I. Gödény, I. A. Szabó, G. Erdélyi, and F. J. Kedves: "On the Diffusion of ^{59}Fe into Aluminum and Al Mn Solid Solutions," *Philos. Mag,* 1987, *55,* pp. 425-443.

1992And: J-O. Andersson and J. Ågren: "Models for Numerical Treatment of Multicomponent Diffusion in Simple Phases," *J. Appl. Phys.,* 1992, *72*(4), pp. 1350-55.

1994Eng: A. Engström, L. Höglund, J. Ågren "Computer Simulation of Diffusion in Multiphase Systems," *Metall. Mater. Trans.,* 1994, *25A*(6), pp. 1127-34.

1994Jon: B. Jönsson, "Assessment of the Mobility of Carbon in fcc C-Cr-Fe-Ni Alloys," *Z. Metallkde,* 1994, *85*(7), pp. 502-509.

1995Jon: B. Jönsson: "Assessment of the Mobilities of Cr, Fe, and Ni in fcc Cr-Fe-Ni Alloys," *Z. Metallkde,* 1995, *86*(10), pp. 686-92.

1996Day1: M.A. Dayananda: "Average Effective Interdiffusion Coefficients and the Matano Plane Composition," *Metall. Mater. Trans.,* 1996, *27A*(9), pp. 2504-2509.

1996Day2: M.A. Dayananda and Y.H. Sohn: "Average Effective Interdiffusion on Coefficients and Their Applications for Isothermal Multicomponent Diffusion Couples," *Scripta Mater.,* 1996, *35*(6), pp. 684-88.

1996Eng: A. Engström and J. Ågren "Assessment of Diffusional Mobilities in Face-Ceneterd Cubic Ni-Cr-Al Alloys," *Z. Metallkde.,* 1996, *87*(2), pp. 92-97.

1996Sau: N. Saunders: "Phase Diagram Calculations for Ni-Based Superalloys," *Superalloys 1996*, R.D. Kissinger,ed., TMS, Warrendale, PA, 1996, p. 101.

1996Wlo: S.T. Wlodek, M. Kelly, and D. Alden: "The Structure of René-88DT," *Superalloys 1996*, R.D. Kissinger, D.J. Deye, D.L. Anton, A.D. Cetel, M.V. Nathal, T.M. Pollock, and D.A. Woodford,ed., TMS, Warrendale, PA, 1996, pp. 129-36.

1998Sau: N. Saunders and A,P. Miodownik, *CALPHAD Calculation of Phase Diagrams: A Comprehensive Guide*, Elsevier Science, New York, 1998.

1999Hel1: T. Helander and J. Ågren: "A Phenomenological Treatment of Diffusion in Al-Fe and Al-Ni Alloys Having B2-BCC Ordered Structure," *Acta Mater.,* 1999, *47*(4), pp. 1141-52.

1999Hel2: T. Helander and J. Ågren: "Diffusion in the B2-BCC Phase of the Al-Fe-Ni System - Application of a Phenomenological Model," *Acta Mater.,* 1999, *47*(11), pp. 3291-3300.

2000Bor: A. Borgenstam, A. Engström, L. Höglund, and J. Ågren: "DICTRA, a Tool for Simulation of Diffusion Transformations in Alloys," *J. Phase Equilibria,* 2000, *21*(3), pp. 269-80.

2001Hog: L. Höglund and J. Ågren: "Analysis of the Kirkendall Effect, Marker Migration and Pore Formation," *Acta Mater.,* 2001, *49* pp. 1311-17.

2002Cam: C.E. Campbell, W.J. Boetttinger, and U.R. Kattner: "Development of a Diffusion Mobility Database for Ni-Base Superalloys," *Acta Mater.,* 2002, *50* pp. 775-92.

2002Zha1: J.C. Zhao, M.R. Jackson, L.A. Peluso, L.N. Brewer: "A Diffusion Multiple Approach for the Accelerated Design of Structural Materials," *MRS Bull.*, 2002, *27*(04), pp. 324-29.

2002Zha2: J.C Zhao, M.R. Jackson, L.A. Peluso, and L.N. Brewer: "A Diffusion Multiple Approach for Mapping Phase Diagrams, Hardness, and Elastic Modulus," *JOM*, 2002, *54* pp. 42-45.

2003Cam: C.E. Campbell, W.J. Boetttinger, T. Hansen, P. Merewether, and B.A. Mueller, "Examination of Multicomponent Diffusion Between Two Ni-Base Superalloys" in *Properties of Complex Inorganic Solids 3,* P.E.A. Turchi, et al., ed., Kluwer Publishers, New York, NY, 2004.

2003DIC: DICTRA (22), 2003, Thermo-Calc AB, Stockholm, Sweden, http://www.thermocalc.com/.

2003Ras: W. Rasband, ImageJ (1.30v), 2003, National Institutes of Health, Besthda, MD, http://rsb.info.nih.gov/ij/.